journal

J. Am. Ceram. Soc., 78 [11] 2929–39 (1995)

Cracking during Pyrolysis of Oxide Thin Films—Phenomenology, Mechanisms, and Mechanics

San-Yuan Chen* and I-Wei Chen*

Materials Science and Engineering, University of Michigan, Ann Arbor, Michigan 48109-2136

Cracking phenomena of oxide ($BaTiO_3$ and $Pb(Zr_{1-x}Ti_x)O_3$) thin films prepared from metal carboxylate and alkoxide solutions were studied. At a higher heating rate and in a reducing atmosphere, cracks formed with a morphology similar to that seen in dried mud or on cracked glazes. At a lower heating rate and in an O_2 atmosphere, cracks formed apparently from degassing bubbles or small crystallites, with a morphology of starlike, short cracks. The critical conditions for these two cracking modes were associated with two transient stress maxima during pyrolysis: first at an intermediate temperature, when the maximum weight loss rate occurred, then toward completion of pyrolysis, as a nearly ceramic state was approached. A viscous stress analysis and fracture energy considerations were used to rationalize the observed scaling relations between critical crack thickness, crack spacing, and processing parameters.

I. Introduction

THERE has been increasing interest in recent years in processing oxide thin films using solution-based methods which include metallorganic decomposition (MOD) and sol–gel processes. In the former process, organometallic compounds dissolved in organic solvent are thermally decomposed after being coated on the substrates.[1–3] In the latter, metal alkoxides dissolved in alcohol are first partially hydrolyzed to form the sols, which can then be coated and heat-treated.[4–5] One attractive feature of these methods is the ability to control precisely the stoichiometry at the molecular level. This is true in the MOD process, which allows direct mixing of feedstocks of individual metallorganic solutions, and in the sol–gel process, which forms a polymerized network with mixed cation species. Other advantages include low processing temperature, fabrication ease, and low cost.

One intrinsic drawback of the solution-based methods is the large volume change from wet chemicals to fired inorganic oxides. Typical ratios of as-deposited to fired film thickness are up to 50 in these processes.[2,6] This volume change can cause cracking in fired films. The tendency for film cracking generally increases with film thickness. Although this difficulty can sometimes be circumvented by using multiple coatings, such practice often results in an inhomogeneous microstructure, since each layer experiences a different thermal history. This, in turn, may affect the crystal structure, grain size, and other aspects of film morphology.[7] Consequently, the development of a thick film in one step is of interest. In addition, it will allow us to identify the critical condition for film cracking and its mechanisms.

Garino[8] has noted that the critical thickness beyond which cracks formed was affected by the annealing temperature and the ratio of water to metal alkoxides used in hydrolysis. In reality, cracking is found to be very sensitive to processing parameters such as the rate of heating and cooling,[2] the firing temperature,[8] the metallo-organic precursors,[4] and the choice of substrates and their surface conditions.[9] Referring to the last parameter, most of the researchers seem to ascribe the problem to thermal expansion mismatch between the film and the substrate.[3,9] This is questionable in view of the large volume reduction during pyrolysis of these films. It is the purpose of this study to identify more positively the controlling parameters that affect cracking and to offer the mechanical origins that cause cracking.

$BaTiO_3$ and $Pb(Zr_{1-x}Ti_x)O_3$ were chosen for this work because of the ease of preparation and potential applications as ferroelectric film devices. Many methods have been developed to prepare crack-free and dense $BaTiO_3$ films.[10] Xu *et al.*[11] have developed an MOD method for making $BaTiO_3$ thin film from barium neodecanoate and titanium dimethoxy-dineodecanoate precursors. This method has been adopted here to prepare $BaTiO_3$ films. For $Pb(Zr_{1-x}Ti_x)O_3$ films, both metal carboxylates and other precursors including metal alkoxides are utilized. The effects of precursor chemistry, feedstock concentration, heating rate, atmosphere, and pyrolyzing temperature on critical thickness and crack morphology, along with characteristics of thermal decomposition and weight changes, are investigated in order to depict the essential elements of cracking phenomenology.

II. Experimental Procedure

(1) *Preparation of Stock Solution*

The precursors used to prepare $BaTiO_3$ were barium neodecanoate ($Ba(C_9H_{19}COO)_2$) and titanium ethoxide ($Ti(OC_2H_5)_4$, 24475-9, Aldrich, Milwaukee, WI), with xylene (C_8H_{10}, 10642-3, Kodak, Rochester, NY) as the solvent. The general procedure utilized to fabricate barium neodecanoate was the same as that of Shaikh and Vest.[12] $BaCl_2 \cdot 2H_2O$ (barium chloride dihydrate, 21756-5, Aldrich) was dissolved in deionized water, and the neodecanoic acid (neodecanoic acid, Exxon Chemicals Americals, Houston, TX) was neutralized with NH_4OH (A-669 S, Fisher Scientific, Pittsburgh, PA). The $BaCl_2$ solution was then slowly added into the ammonium soap solution, using a separator funnel with vigorous stirring to effect the following reactions:

$$NH_4OH + C_9H_{19}COOH \rightarrow C_9H_{19}COONH_4 + H_2O \quad (1)$$

$$2C_9H_{19}COONH_4 + BaCl_2 \rightarrow Ba(C_9H_{19}COO)_2 + 2NH_4Cl \quad (2)$$

The barium neodecanoate that formed was a white gummy substance which could be separated from the aqueous layer. The concentration and viscosity of the resultant mixture of an equimolar amount of barium and titanium solutions were adjusted by adding xylene. A solution with 15.2 wt% of $BaTiO_3$, having a viscosity of 3.2 cps, was used in most of our experiments unless otherwise noted.

An MOD procedure parallel to the above was also developed for $Pb(Zr_{1-x}Ti_x)O_3$ feedstocks. The wet chemistry was reported in our previous publication.[13] The final substances obtained were lead 2-ethylhexanoate ($Pb(C_8H_{15}O_2)_2$, 89308, Alfa,

A. Jagota—contributing editor

Manuscript No. 193061. Received November 8, 1994; approved June 12, 1995.
Supported by the U.S. Department of Energy—Basic Energy Sciences under Grant No. DE-FG02-87ER45302.

*Member, American Ceramic Society.

Ward Hill, MA), zirconium 2-ethylhexanoate ($Zr(C_7H_{15}COO)_4$, Z01373, Pfaltz and Bauer, Waterbury, CT), and titanium diethoxydineodecanoate ($Ti(OC_2H_5)_2(C_9H_{19}COO)_2$). The precursor obtained by mixing the above is referred to later as A.

We also investigated films obtained from other precursors. In precursor B, titanium ethoxide was used, while the rest of the feedstocks were the same as in A. In precursor C, zirconium *n*-propoxide ($Zr(O(CH_2)_2CH_3)_4$, 22989, Alfa) was used, while the rest were the same as in B. In precursor D, lead acetate trihydrate ($Pb(CH_3CO_2)_2 \cdot 3H_2O$, 87922, Alfa) was used, while the rest were the same as in C. In addition, precursor D was refluxed at around 120°C for 5 h and then distilled at 105°C to remove byproducts, following the sol–gel procedure of Budd *et al.*[4] before casting thin films.

(2) Fabrication of Thin Films

Two kinds of substrates were used in this study: an Si(100) wafer and a Pt(111)/Ti/SiO_2/Si substrate. The Si wafer was covered by a layer of native oxide, while the thickness of Ti was about 20 nm and that of Pt was about 150 nm. Thin films were fabricated on the substrates by spin coating. For $BaTiO_3$ films, the spinning condition used was 1000–6500 rpm for 20 s to produce films of different thicknesses. After deposition, the films were first dried at 150°C for 30 min to evaporate xylene and then pyrolyzed at 550°C for 30 min. Different heating rates of 1°–35°C/min were used in the latter process. Fast heating experiments which placed thin films into a tube furnace with a preset temperature were also conducted. After pyrolysis, the films were allowed to cool to room temperature with furnace cooling. To investigate the effect of atmosphere, air, O_2, and 5%H_2–95%N_2 (later referred to as N_2/H_2) were used in the pyrolysis. For $Pb(Zr_{1-x}Ti_x)O_3$ films, the conditions were similar to the above, except the as-deposited films were pyrolyzed at 450°C for 30 min in air.

(3) Characterization of Solutions and Thin Films

The barium content in the barium neodecanoate was determined by precipitating $BaSO_4$ in a weighed sample with hot, dilute sulfuric acid. The titanium content of the titanium ethoxide was determined by hydrolyzing preweighed samples in ammonia and calcining the precipitated material into TiO_2 at 730°C.[14] Similar calcination procedures were used to determine the content of Pb, Zr, and Ti feedstocks.[13] The accurate stoichiometric ratio of Ba to Ti and Pb to Zr to Ti was then adjusted to formulate the solution. The viscosity of the mixture solutions was measured using a viscometer (Brookfield Model DV-II). The thermal behavior of the solutions was studied by using simultaneous thermogravimetric analysis (TGA) and differential thermal analysis (DTA). All thermal analyses were done at a heating rate of 1°–35°C/min in the atmosphere of air, O_2, and N_2/H_2. The final products were characterized by X-ray diffraction (XRD) with Cu$K\alpha$ radiation. The microstructure and crack morphology of thin films were further examined by using optical microscopy and scanning electron microscopy (SEM). The mean intercept length of a random test line was then used to measure crack spacing from 3–5 cracked films. A Dektak II profilometer was used to measure the thickness of the pyrolyzed films on the substrates. To determine the critical thickness of pyrolyzed film required for cracking, 3–5 samples that barely formed cracks were measured to obtain their average thickness. (See also Fig. 6 caption.)

In the following, we will give a detailed description of the results obtained for $BaTiO_3$ (BT) films. The main findings are similar for $Pb(Zr_{1-x}Ti_x)O_3$ (PZT) films, so the description is abbreviated except when needed for pointing out significant differences.

III. Results

(1) Characterization of Solutions

Figure 1 shows the thermograms of the solution of an equimolar mixture of barium neodecanoate and titanium ethoxide (BT). There are two important weight loss stages in Fig. 1(a). The first stage, around 120°C, results from the evaporation of solvent (xylene). The second stage, extending between 180° and 500°C, originates from the removal of the carboxylate groups. At the lowest heating rate (1°C/min), most of the weight loss with the carboxylate groups occurred in a narrow temperature range, from 300° to 360°C, giving rise to a violently exothermic peak at 350°C in the DTA (Fig. 1(b)). An exothermic shoulder around 580°C was also detected; no weight loss was seen at this stage. XRD found the formation of $BaCO_3$ starting at 320°–350°C and later $BaTiO_3$ at 590°C, the latter being responsible for the DTA shoulder at 580°C. The XRD signal of the TiO_2 phase was usually too weak to be observed.

The thermograms of solutions of barium neodecanoate with titanium ethoxide are affected by atmospheres, as shown in Fig. 2. The major stages of weight loss remain the same in all atmospheres, but the completion temperatures are delayed as the atmosphere changes from O_2/air to N_2/H_2. The thermograms, however, have very different characteristics under oxidizing and reducing atmospheres. In both O_2 and air, a strong exothermic DTA peak at around 300°–360°C accompanies the steep weight loss at this stage. This was followed by a broad exothermic peak at 570°C (without weight loss), again attributed to the formation of $BaTiO_3$. The DTA curve for the N_2/H_2 atmosphere shows a completely different picture. The weight loss at the intermediate temperature was now accompanied by a broad endothermic peak around 350°C. Another minor endothermic peak was also seen around 500°C. The latter is probably due to the carburization of remaining carboxylate groups as evident from the dark color of the powder. Thus, the evaporation and decomposition of neodecanoate group is intrinsically endothermic but can be exothermic and accelerated when aided by oxidation.

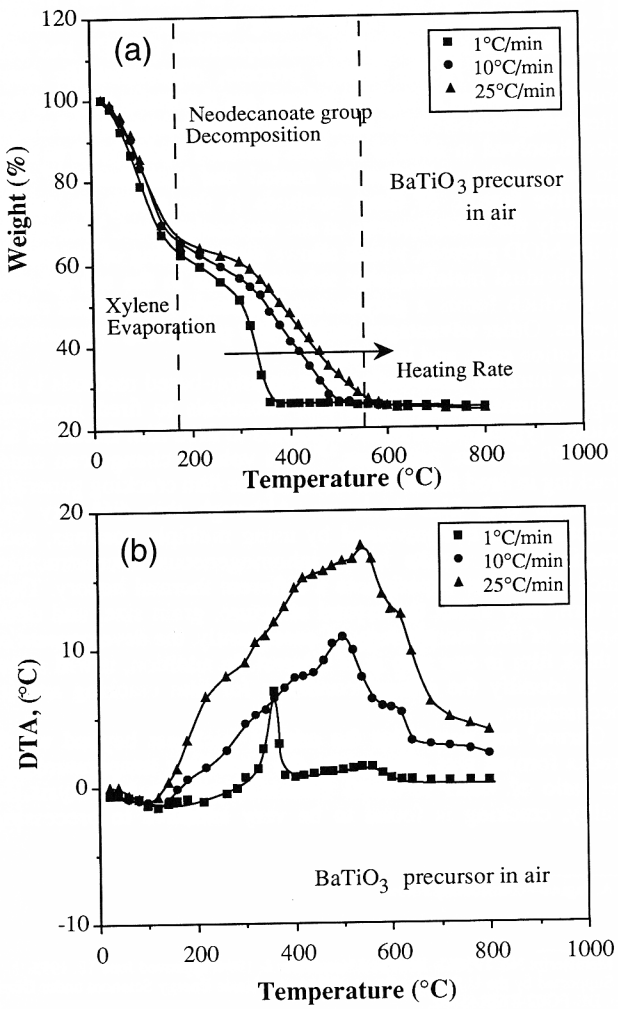

Fig. 1. (a) TGA and (b) DTA of $BaTiO_3$ precursor heated at different rates in air.

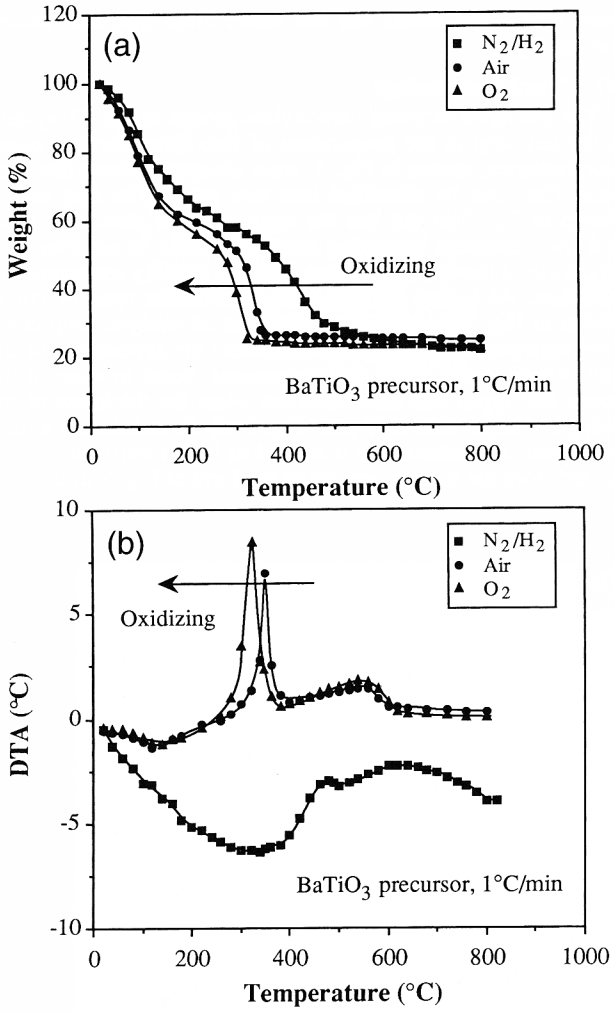

Fig. 2. (a) TGA and (b) DTA of $BaTiO_3$ precursor heated in different atmospheres at 1°C/min.

X-ray patterns of various precursor solutions establish the following. When slowly pyrolyzed in air, the final products are TiO_2 (anatase and rutile) in the case of titanium ethoxide above 400°C, $BaCO_3$ in the case of barium neodecanoate above 320°C, and $BaCO_3$ in the case of titanium ethoxide and barium neodecanoate mixture up to 550°C. Complete transformation to $BaTiO_3$ in the latter case can be achieved by heating to 600°C. These thermal reactions are influenced by the atmospheres. For $BaTiO_3$ film on Si substrate, the X-ray pattern of films pyrolyzed in air and O_2 at 550°C for 0.5 h shows only the $BaCO_3$ phase. At 400°C in air, $BaCO_3$ peaks become noticeable after 0.5 h. The sample pyrolyzed in N_2/H_2 at the same temperature is apparently amorphous. It should be noted that cracking usually developed before or at 550°C. Uncracked films pyrolyzed to 550°C were not cracked during subsequent calcination into $BaTiO_3$.

The thermogram and crystallization sequence of PZT films prepared from precursor A have been reported in a previous publication[13] and are not repeated here. Other precursors behave qualitatively the same except for shifts of temperatures and rates of pyrolysis. Later, in Section IV(4), we will return to this point to relate it to cracking mechanisms.

(2) Effect of Heating Rate

At increasing heating rate, both the weight loss and the exothermic peak spread out. The temperature when pyrolysis is complete, as indicated by the saturation of weight loss, increases with heating rate. This temperature is denoted as T_{100} and plotted in Fig. 3. Likewise, the temperature when pyrolysis weight loss rate is the largest, corresponding to the inflection point in the middle temperature range of Fig. 1(a), is slightly

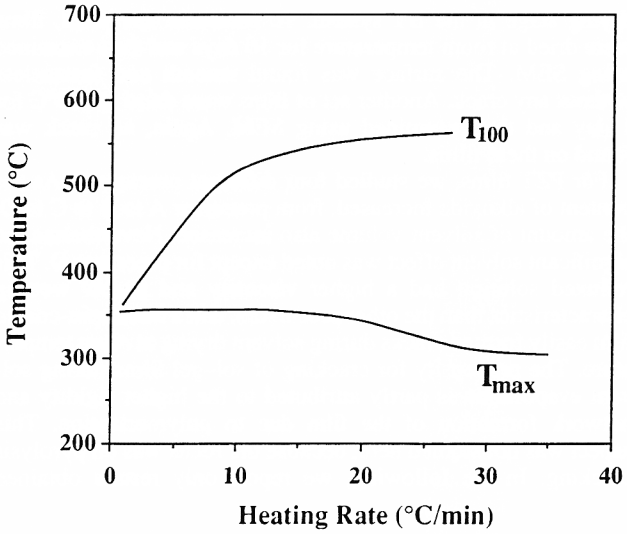

Fig. 3. Temperature when full relative density is reached (T_{100}) and when maximum weight loss rate is experienced (T_{max}) for a $BaTiO_3$ precursor.

dependent on the heating rate. This temperature is denoted as T_{max} and also plotted in Fig. 3. Note that the weight loss rate, which is the product of the slope of Fig. 1(a) and the heating rate, increases monotonically with the heating rate. In this sense, the exothermic weight-loss reaction in the intermediate temperature range is actually more "violent" at a higher heating rate, despite the more spread-out appearance in Figs. 1(a–b).

(3) Effect of Feedstock Concentration on Film

The thickness of a deposited layer is a function of the solution viscosity, spinning speed, and time. For $BaTiO_3$ fims, the solution viscosity and initial volume reduction during drying were controlled by using a xylene solvent. However, we found that the solvent had almost no influence on film cracking in this system. As shown in Fig. 4, the film thickness (after pyrolysis using 10°C/min to 550°C in air) decreases with increasing spinning speed and with decreasing viscosity, which corresponds to a higher content of solvent and a larger initial volume reduction. The critical thickness beyond which cracking was found is also indicated in Fig. 4 by the broken line and seems to remain constant. Thus, the different initial volume reduction has little influence on the critical thickness. The maximum critical thickness is always around 0.38–0.48 μm. This implies that cracking is controlled by pyrolysis and not influenced by the solvent-

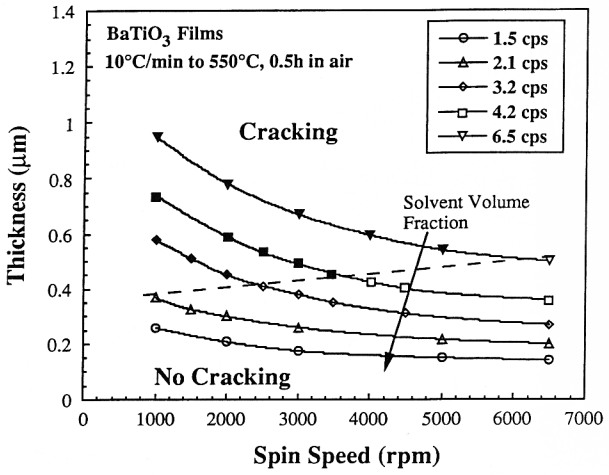

Fig. 4. Film thickness after pyrolysis at 550°C in air for 0.5 h. The thickness depends on spin speed and precursor viscosity, which can be adjusted by solvent addition. Cracking is observed in thicker films (closed symbols), but not in thinner films (open symbols).

drying stage in the BT system. To ascertain this point, films were dried at room temperature for 10 days and then examined using SEM. The surface was found smooth and featureless without any crack. Another set of films were dried at 150°C for 1 day and then examined using SEM. Again, no crack was found on these films.

For PZT films, we studied four different precursors. As the content of alkoxide increased, from precursor A to B to C to D, the amount of solvent volume also increased. Nevertheless, no significant solvent effect was noted except for precursor D. This refluxed solution had a higher viscosity and poorer wetting characteristics than the other precursors, and a thick spin-coated film easily formed cracks during solvent drying at room temperature. The propensity for cracking of sol–gel films during solvent evaporation is partly attributed to the higher rigidity and network formation of the film due to polymerization. This aspect was not studied here, because the focus was on pyrolysis cracking. In the following, we report only results obtained from PZT films which did not suffer from cracking during solvent drying.

(4) Crack Morphology

The pyrolysis of metal carboxylate groups in the BT system is the key step in the preparation of thin films. Several crack morphologies, shown in Fig. 5, were observed during this process. They can be classified into two types. The first one is shown in Fig. 5(a) and has the appearance of stars with short and wide openings branching from the center. In air, they usually occur at lower heating rates and give a milky appearance to the films. At higher heating rates, a different type of crack, shown in Fig. 5(b), with an appearance of straight, long crack lines appears. These cracks do not affect the appearance of the film, which is still shiny and transparent. Some mixture of the above two types was also observed when the thickness of the film grew larger than 0.55 μm (Fig. 5(c)). In addition, if a fully pyrolyzed, uncracked film is cooled to liquid nitrogen or fast-cooled from the furnace, cracks of the form of Fig. 5(d) develop

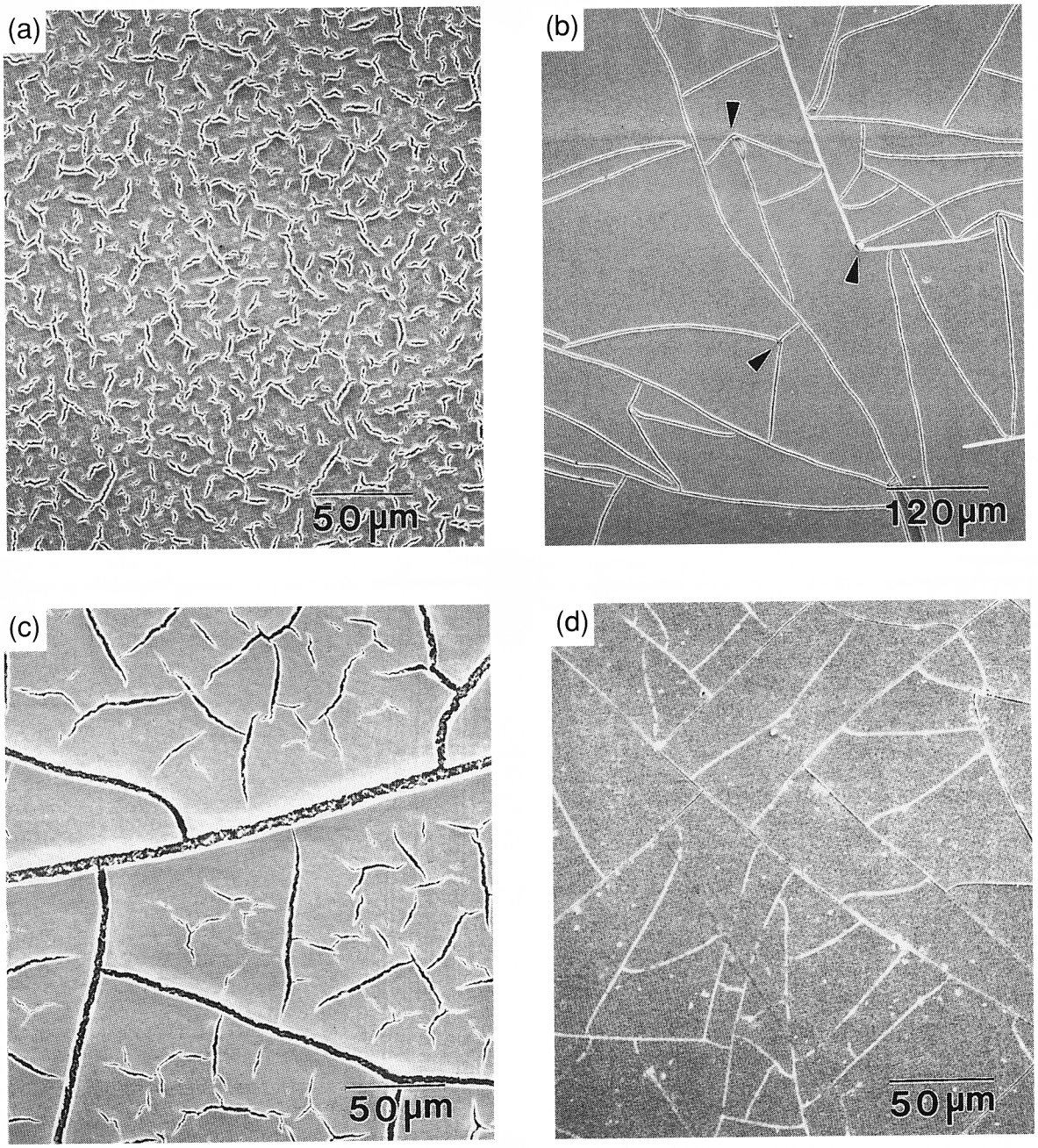

Fig. 5. Morphology of cracks found in pyrolyzed BT films: (a) type II cracks, (b) type I cracks, (c) mixed cracks, and (d) thermal shock cracks. Crack origins at dust or foreign particles are marked in (b).

at the thicker section. These cracks in Fig. 5(d) are almost certainly due to the tensile stress in the films, because silicon is known to have a much smaller thermal expansion coefficient than $BaTiO_3$. The appearance of these cracks bears some resemblance to the cracks in Fig. 5(b), except that they are more straight and narrow.

We investigated the effect of atmosphere on the morphologies of these cracks in the BT system. In the reducing atmosphere (N_2/H_2), only the long, network cracks shown in Fig. 5(b) were observed. Thus, the other cracks (Fig. 5(a)) must be due to oxidation. It is possible that the center of these starlike cracks corresponds to a degassing bubble or inclusion (such as a crystallite) that causes concentration of internal stress, facilitating cracks emanating from it. The density of this type of crack is much higher in O_2 than in air at comparable film thickness. The other cracks with a network appearance, Fig. 5(b), bear some similarity to those seen in dried mud or on cracked glaze. In the following, we will refer to the cracks of Fig. 5(b) as type I and those of Fig. 5(a) as type II. Finally, cracks seen in Fig. 5(d) are clearly due to thermal expansion mismatch and will hereafter be termed thermal shock cracks. We will return to the cracking mechanisms in a later section.

(5) Critical Thickness

As mentioned in the Introduction, there is a critical thickness of film beyond which cracks form. The critical thickness was determined first for BT films pyrolyzed in air heated at different rates. As shown in Fig. 6, this thickness reaches a maximum of around 0.42 μm at an intermediate heating rate of 10°–15°C/min for films made from a solution with a viscosity of 3.2 cps. This optimal condition between critical thickness and heating rate also exists in films prepared from other solutions in the BT system.

In Fig. 6, we have also outlined the regions for different crack types. At lower heating rates, type II cracks (Fig. 5(a)) dominate at lower thickness and mixed cracks (Fig. 5(c)) dominate at higher thickness. On the other hand, type I cracks (Fig. 5(b)) dominate at higher heating rates. This trend is again found for other BT solutions.

The effect of atmosphere on critical thickness of BT films is seen in Fig. 7. At lower heating rates, a reducing atmosphere is beneficial for obtaining a larger critical thickness. Indeed, the maximum thickness which a BT film can reach without cracking is around 0.47 μm at a heating rate of 1°C/min in N_2/H_2 atmosphere. Conversely, if O_2 is used in pyrolysis, the critical thickness is drastically reduced at lower heating rates. The maximum thickness obtained in O_2 is only about 0.3 μm and only at relatively high heating rates above 20°C/min. Note that only type II cracks are seen in O_2 pyrolysis, whereas only type I cracks are seen in N_2/H_2 pyrolysis.

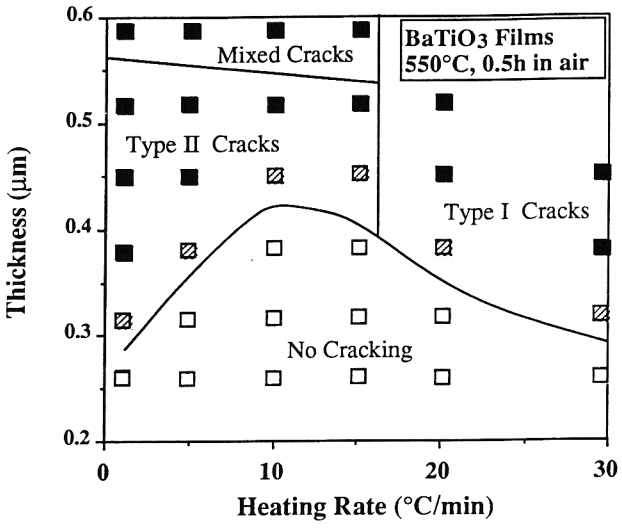

Fig. 6. Critical thickness of BT films pyrolyzed at 550°C in air for 0.5 h at different heating rates. Cracks of different morphologies as indicated are observed in thicker films (closed symbols), but not in thinner films (open symbols). Shaded symbols indicate that cracking is sometimes observed. The curve of critical thickness is drawn between open and shaded symbols, with the location chosen to reflect the cracking statistics of the shaded-symbol data.

(6) Starting Temperature and Time for Crack Formation

The starting temperature and time for crack formation were determined using the following heating schedule. The films were heated at various heating rates to a set temperature, then furnace-cooled immediately without soaking. The temperatures when the cracks first appeared (by light microscopy examination) in BT films are shown in Fig. 8 for two different thicknesses. We found that the starting temperature for crack formation was the highest at an intermediate heating rate, and the thicker film had a lower starting temperature for crack formation. As in Fig. 6, different cracks are predominant at different heating rates. Type II cracks (open symbols) form at lower heating rates, with the starting temperature increasing with increasing heating rate. This tendency is reversed for the case of type I cracks (full symbols), which form at higher heating rates with the starting temperatures decreasing with increasing heating rates. In thinner films under the condition of a constant heating rate, the first formation of type I cracks was never followed by the formation of type II cracks. This is indicated in Fig. 8 by the absence of oxidation cracks at higher temperatures in 0.41 μm film. Likewise, the first formation of type II cracks under a constant heating rate in the thinner films was not followed by the formation of type I cracks, as indicated in Fig. 8 by the absence of type II cracks at higher temperatures in 0.41 μm film. In thicker film, though, both type I and II cracks (i.e., mixed cracks) can be seen, as indicated in Fig. 8, for 0.55 μm films at lower heating rates. The micrograph shown in Fig. 5(c) reveals that, in such a case, the crack opening is much wider for type I cracks than for type II cracks. Assuming a large part of the crack opening comes from volume shrinkage subsequent to crack formation, this observation would imply that type I cracks formed before type II cracks. The following experiment further established that this is indeed the case.

To determine the pyrolysis time required for crack formation at various temperatures in air, dried (150°C for 30 min) films were placed into a furnace at a preset temperature for a certain time, followed by furnace cooling. The final film thickness was about 0.55 μm after full pyrolysis. The results in Fig. 9 show a longer time required to form type II (mixed) cracks than type I cracks. At lower temperatures, the time lag is longer, reflecting the slower speed of pyrolysis. The time required for forming

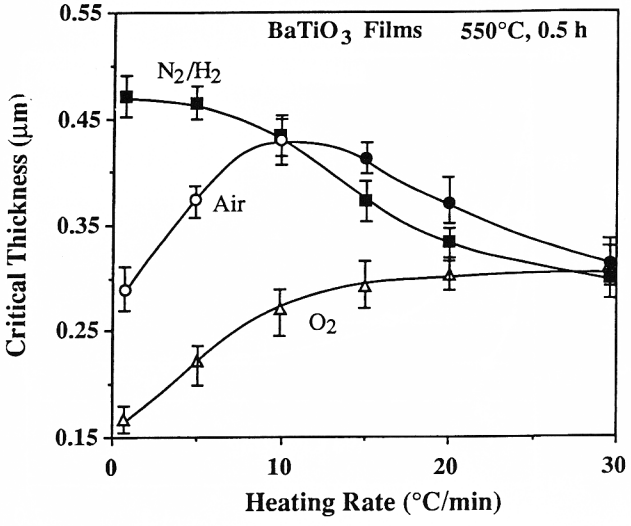

Fig. 7. Effect of atmosphere on critical thickness for BT films pyrolyzed at 550°C for 0.5 h at different heating rates. Closed symbols indicate type I cracks, and open symbols indicate type II cracks when critical thickness is exceeded.

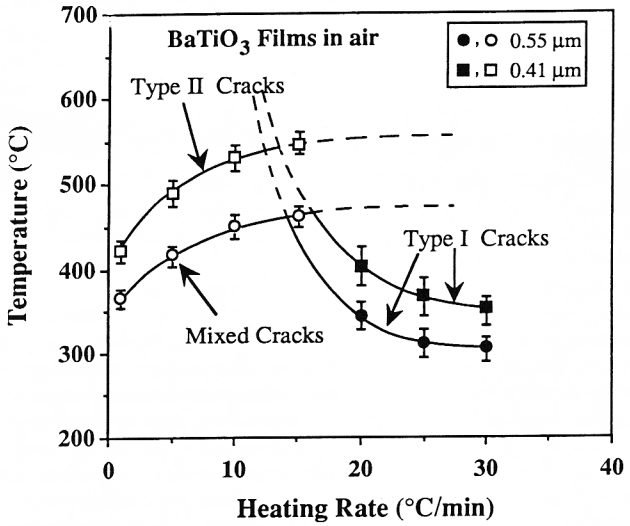

Fig. 8. Starting temperature for crack formation in BT films of two thicknesses pyrolyzed in air at different heating rates.

type II (mixed) cracks roughly corresponds to that required for $BaCO_3$ formation. For example, the XRD signal of $BaCO_3$ was seen after 0.5 h at 400°C, comparable to that shown for mixed cracks in Fig. 9. Also, no crack forms below 280°, even for a very long holding time. The above threshold temperature seems to correspond to the onset of the steep second stage weight loss in Fig. 1(a), which occurs at around 320°–350°C.

For BT films, we have experimented with various soaking times at 550°C and various cooling rates after air pyrolysis at this temperature. It was found that these parameters have essentially no influence on the cracking tendency and crack density. This is consistent with Fig. 9, which indicates that both type I and type II cracks should form very quickly in the film at 550°C if the film thickness is beyond critical. Therefore, despite the possibility of some thermal shocks in the extreme cases, e.g., Fig. 5(d), it is the heating step and pyrolysis that hold the key for crack formation in these films.

(7) Crack Spacing

We measured the crack spacing using the linear intercept method. The data are plotted in Figs. 10 and 11. Denoting crack spacing as λ, film thickness as h, and heating rate as R, type I cracks (full symbols) follow λ–$h^{-0.83}R^{-0.59}$ and type II cracks (open symbols) follow λ–$h^{-0.83}R^{0.37}$. It is remarkable that crack

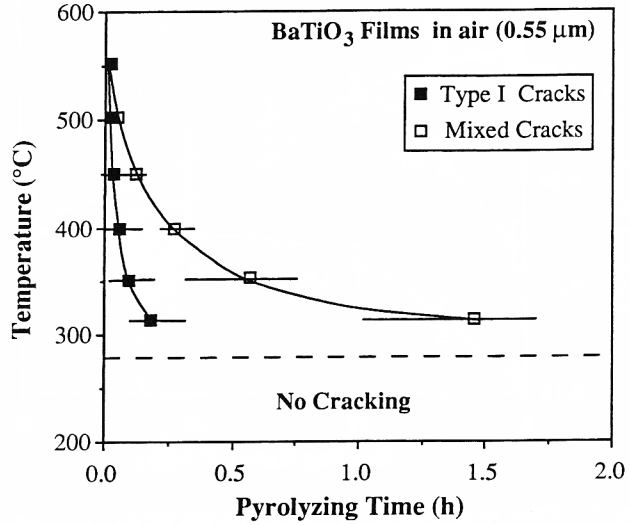

Fig. 9. Starting time for crack formation in BT films (0.55 μm) pyrolyzed in air at different temperatures.

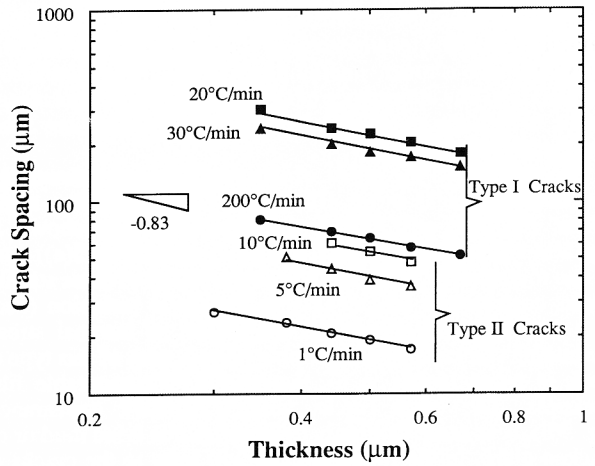

Fig. 10. Crack spacing vs film thickness in BT films for type I cracks (closed symbols) and type II cracks (open symbols) at different heating rates.

spacing decreases with film thickness in contrast to several previous experimental reports on thermal/elastic stress cracking[15,16] and gel-drying cracking.[17,18] The above scaling relations will be discussed in a later section.

(8) PZT Films—The Influence of Precursor Chemistry

The morphology of pyrolysis cracks in PZT films is qualitatively similar to that in BT films. As shown in Fig. 12, two types of crack morphologies corresponding to type I cracks (Fig. 12(a)) and type II cracks (Fig. 12(b)), both taken from precursor B, are evident. Interestingly, only type II cracks were seen in films made from precursor A, with morphologies very similar to those of Fig. 12(b). In contrast, only type I cracks were seen in films made from precursor C and D, with morphologies very similar to those of Fig. 12(a).

Critical thickness for crack formation was also studied. For PZT films heated at various heating rates to 450°C and held for 0.5 h, the results are shown in Fig. 13. Data points on curves which have a rising slope are found to correspond to type II cracks (open symbols), whereas those with a falling slope correspond to type I cracks (full symbols). These results are the same as that seen for BT films. Note that, although the chemistry of precursors varies systematically from A to B to C to D, the variation of the critical thickness is not in the same order.

As a practical matter, PZT films are used for various applications. The preferred method of pyrolysis often involves fast heating. The critical thickness for films heat-treated in such a

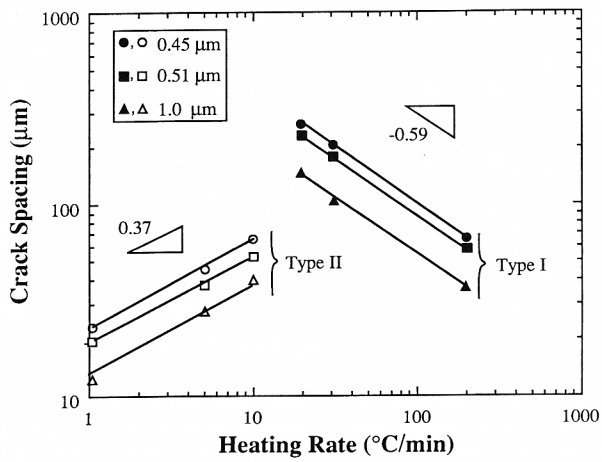

Fig. 11. Crack spacing vs heating rate in BT films for type I cracks (closed symbols) and type II cracks (open symbols) for different film thickness.

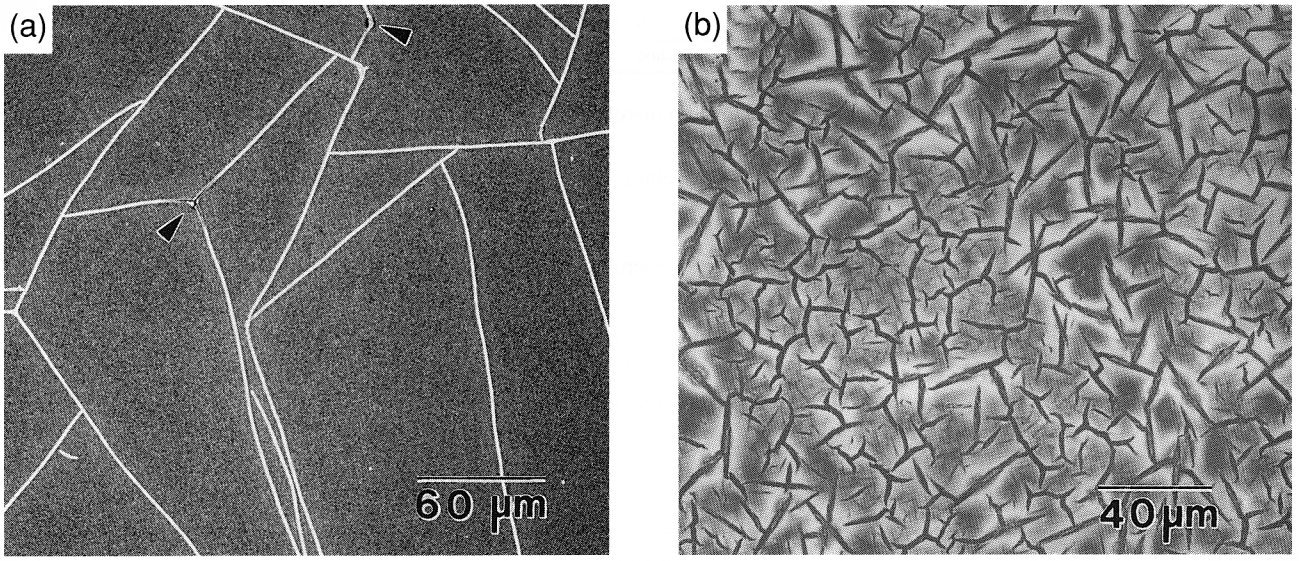

Fig. 12. Morphology of cracks found in pyrolyzed PZT films (B precursor): (a) type I cracks, (b) type II cracks. A crack origin at a dust particle is marked in (a).

way (estimated heating rate at 200°C/min in our experiment) is indicated on the far right of Fig. 13. We also noticed some compositional effect in PZT films prepared from precursor B. The Ti-rich compositions tend to form type I cracks, but Zr-rich compositions tend to form type II cracks. It should be noted that the Zr-rich compositions pyrolyze slower,[19] as indicated by the higher temperature for the second weight loss stage.[4] As reported by Budd *et al.*,[4] the large exothermic peak corresponding to the complete weight loss was approximately at 300°C for $PbTiO_3$ gels and near 500°C for $PbZrO_3$ gels. The relevance of this aspect to the cracking tendency will be discussed later (Section IV(4)).

IV. Discussion

(1) Thermal Decomposition of $BaTiO_3$ Solutions

The weight loss of $BaTiO_3$ solution consists primarily of two steps. One results from the evaporation of xylene solvent, and the other, starting from around 200°C, termed pyrolysis, is associated with the decomposition and evaporation of carboxylate groups. The latter step could be either exothermic or endothermic, depending on whether oxidation occurs. The heating rate and atmosphere have little influence on xylene evaporation, but markedly affect the rate of weight loss during the second step. Apparently, the heating rate and the oxygen activity affect the reaction kinetics of organic removal and the temperature of decomposition. The completion temperature of weight loss is generally delayed with increasing heating rate and decreasing oxygen activity.

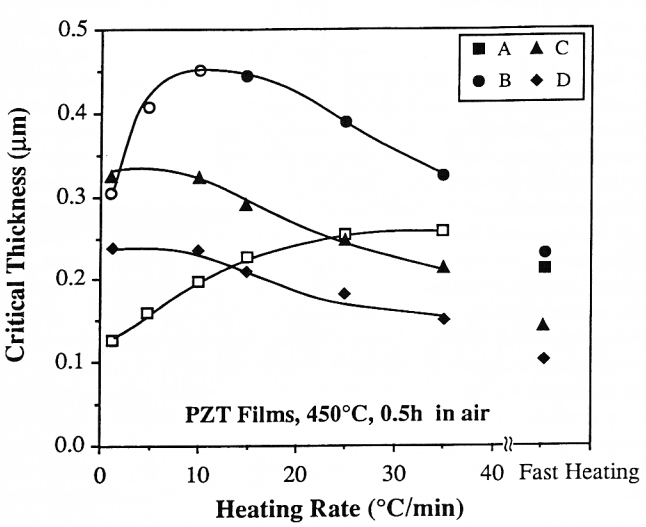

Fig. 13. Critical thickness of PZT films pyrolyzed at 450°C in air for 0.5 h at different heating rates. Closed symbols indicate type I cracks, and open symbols indicate type II cracks when critical thickness is exceeded.

The physico-chemical reactions are summarized in Table I. Without oxygen, the anaerobic decomposition of the Ba-neodecanoate and titanium ethoxide mixture solution in N_2/H_2 is probably due to the gradual breakup of the carbon chains and the evaporation of the low molecular weight products. Evidence for the latter can be seen in the broad endothermic peak at around 350°C in Fig. 2 and causes a weight loss of 37 wt%. The secondary endothermic peak at 500°C is due to the carburization of the remaining carboxylate salt to form a carbonaceous residue as evidenced by the dark color of the powder. This causes a weight loss of 6 wt%. Budd *et al.*[4] reported that all of the major exothermic peaks in oxygen pyrolysis were replaced by mild endotherms when pyrolyzed in a reducing atmosphere for Pb-Zr-Ti precursors. This is similar to our finding. In an atmosphere of air or O_2, the violently exothermic reactions probably mask any small endothermic decomposition processes over this temperature range. The difference in completion temperature for weight loss may be attributed to the exothermic nature of the strong oxidation reaction which accelerates decomposition. Examples of this effect are abundant in the literature. In the decomposition of anhydrous acetate salt in N_2, an endothermic instead of exothermic peak has been seen, and the completion temperature of decomposition of acetate salt is delayed by 100°C.[20] A similar influence of atmospheric control on the pyrolysis of organic solution was reported by Lipeles *et al.*[21] for the sol–gel solution of lead zirconate titanate.

Crystallization in this system also appears in two steps. During slow heating, $BaCO_3$ phase of poor crystallinity begins to form around 320°–350°C in oxidizing atmospheres. This corresponds to the sharp exothermic peak in the DTA curves in air or O_2. Essentially, no further weight loss was detected beyond these temperatures, and an inorganic mass was obtained. Also in oxidizing atmospheres, the solid-state crystallization of $BaTiO_3$ occurs around 580°C according to DTA and XRD, and $BaCO_3$ has completely disappeared above 600°C. In

Table I. Summary of Thermal Analysis for $BaTiO_3$ Solution

	Reaction	Temperature	ΔH	ΔW (%)
Ba-neodecanoate	Xylene evaporation	RT–120°C	+	25
	Neodecanoate decomposition (aerobic)	250°–540°C	−	48
Titanium ethoxide	Ethanol evaporation	75°–200°C	+	52
	Ethoxide decomposition (aerobic)	200°–400°C	−	21
$BaTiO_3$ solution				
Air (1°C/min)	Xylene evaporation	RT–160°C	+	33
	Neodecanoate decomposition (aerobic)	160°–360°C	−	42
	BT crystallization	560°–600°C	−	0
Air (25°C/min)	Xylene evaporation	RT–200°C	+	30
	Neodecanoate decomposition (aerobic)	200°–580°C	−	44.9
O_2 (1°C/min)	Xylene evaporation	RT–160°C	+	35
	Neodecanoate decomposition (aerobic)	160°–320°C	−	41.7
	BT crystallization	550°–600°C	−	0
5%H_2–95%N_2 (1°C/min)	Xylene evaporation	RT–180°C	+	31
	Neodecanoate decomposition and evaporation (anaerobic)	180°–450°C	+	37
	Neodecanoate carburization	450°–550°C	+	6

a reducing atmosphere, $BaCO_3$ does not form at 550°C from XRD, but probably begins to appear at higher temperature. The XRD pattern of 750°C N_2/H_2 pyrolyzed film, however, shows a mixture of $BaCO_3$ and $BaTiO_3$. Therefore, the conversion to $BaTiO_3$ is very sluggish in this case.

The above considerations are relevant to the investigation of crack formation mechanisms. Concerning decomposition reactions, it is the carboxylate group in the second weight loss stage that is the dominant consideration in the crack-forming process. Concerning crystallization, we believe $BaTiO_3$ plays no role in film cracking, because in both oxidizing and reducing atmosphere, cracking ocurs below 550°C, when $BaTiO_3$ is not yet formed. The formation of $BaCO_3$, though, seems critical for type II cracks, as will be discussed next.

(2) Cracking Conditions for Thin Films

The two morphologies of pyrolysis cracks observed here have also been reported in the literature. Type I cracks have been observed in $BaTiO_3$ thin film using the MOD method.[7] Type II cracks have been observed in $YBa_2Cu_3O_{7-x}$ films prepared from a sol–gel solution[22] and metallo-organic decomposition.[23] Apparently, they are quite common for pyrolyzed oxide thin films, and their formation is probably due to similar causes.

The present study positively identifies the different pyrolysis conditions for the two cracking modes. Type I cracks are favored in reducing atmospheres, at faster heating rates, at shorter times, and in the absence of any crystallized phase, whereas type II cracks are favored in oxidizing atmospheres, at lower heating rates, at longer times, and in the presence of some crystallized phase, e.g., $BaCO_3$. (The influence of precursor chemistry will be postponed to Section IV(4).) The formations of these two types of cracks are often mutually exclusive, especially in thinner films, suggesting two independent sources of stress development for which the requisite conditions do not coexist. Careful examination of the micrographs further shows that the fracture origins of type I cracks are usually some dust or foreign particles (see Fig. 5 at positions marked by arrows), but fracture origins of type II cracks are too numerous to be attributed to such objects and must be due to intrinsic features in the microstructure such as small crystallites ($BaCO_3$, PZT, or pyrochlore), or gas bubbles formed within the film.

To appreciate the origin of stresses that cause cracking, consider the substrate to remain rigid so that the film stress developed during pyrolysis is given by

$$\sigma \approx \eta\dot{\varepsilon} \tag{1}$$

In the above, σ is the tensile stress, $\dot{\varepsilon}$ is the strain rate, and η is the viscosity. In a pyrolyzing thin film, the strain rate is related to the rate of weight loss plus the rate of sintering and is thus dependent on pyrolysis conditions (temperature, atmosphere, and heating rate). Meanwhile, η is sensitive to the ceramic/organic content, porosity, and temperature. In addition, in the post pyrolysis sintering stage, the stress is ultimately dictated by the sintering stress and is inversely related to the pore radius. Thus, the stress development is necessarily complicated. A simplified view adopted here is to assume that a temporal stress maximum is experienced when $\dot{\varepsilon}$ or η goes through a maximum itself. This argument is developed further below and shown to be capable of explaining the cracking phenomena.

Since the maximum strain rate occurs at T_{max} according to Fig. 3, a transient stress maximum σ_{max} is also experienced at T_{max}. For the film viscosity, we expect it to go through a maximum when pyrolysis is nearly complete, i.e., near T_{100}. This is because below T_{100} the viscosity is lower due to remaining organics, while above T_{100} the viscosity is lower due to thermal softening. The corresponding transient stress maximum at around T_{100} is denoted as σ_{100}. (At much higher temperatures the magnitude of viscosity eventually becomes insignificant, because the stress diminishes to approach that of the sintering pressure, while the rate of weight loss is zero.) Cracking can occur at either of these two temporal stress maxima if they exceed the critical stress[24] of a film of a thickness h:

$$\sigma_c \approx K_{IC}/h^{1/2} \tag{2}$$

In the above, K_{IC} is the fracture toughness of the film.

The stress magnitude of σ_{100} and σ_{max} is schematically delineated in Fig. 14 as a function of heating rate to make contact with Fig. 3. Here σ_{100} is shown to decrease with heating rate, because of thermal softening of viscosity. In contrast, σ_{max} is shown to increase with heating rate, because the magnitude of the maximum weight loss rate increases with the heating rate, as noted in Section III(2). It is seen that, at low heating rates, films crack when $\sigma_{100} \geq \sigma_c$; at high heating rates, films crack when $\sigma_{max} \geq \sigma_c$. Since σ_c increases with decreasing film thickness according to Eq. (2), thinner films can avoid cracking, especially at intermediate heating rates, whereas thicker films always crack one way or the other. This prediction is in qualitative agreement with our observations.

Further quantitative comparison can be made by referring to a marginal thickness which is just sufficient for the film to experience cracking at all heating rates (i.e., $h = h_2$ in Fig. 14). Referring to Fig. 6, this thickness is 0.41 μm when the $BaTiO_3$ film is pyrolyzed in air. In Fig. 15 we plot the temperatures where cracking was first observed in this film (the data are the same as those in Fig. 8) and compare them with T_{100} and T_{max} taken from Fig. 3. The first cracking temperatures are found to lie just above T_{100} and T_{max}, at low and high heating rates, respectively. (The fact that T_{100} and T_{max} lie below the data point is reasonable, since experiments were performed at 10°C intervals, so the data point, by necessity, overestimates the first cracking temperature. In addition, we have found the various characteristic temperatures for thermal decomposition estimated from TGA experiment to be systematically lower than those required for the thin-film pyrolysis.) This suggests that at

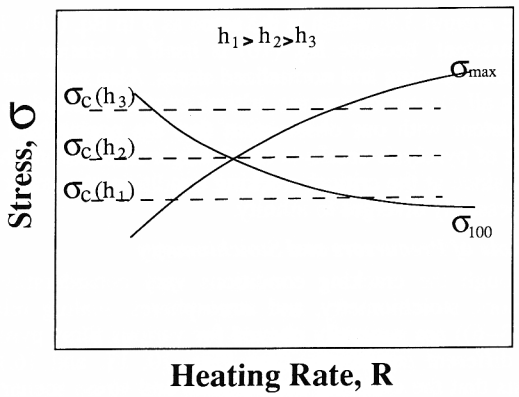

Fig. 14. Schematic dependence of stress on heating rate. σ_{100} is the stress at T_{100}, and σ_{max} is the stress at T_{max}. Cracking occurs when $\sigma \geq \sigma_c$, which decreases with film thickness h.

higher heating rates type I cracks appear when maximum weight loss rate is experienced, whereas at lower heating rates type II cracks occur when pyrolysis is nearly complete.

The above scenario can also explain several other observations. First, since the maximum weight loss rate always occurs before full relative density is reached, it is reasonable that, when both types of cracking occur, type I cracks appear before type II cracks (see Fig. 9). Second, for thicker films, σ_c is already exceeded before stress maxima are reached. Thus, the first cracking temperature should be lower than T_{max} for type I cracks and T_{100} for type II cracks (see Fig. 8). Third, for film pyrolyzed in a less oxidizing atmosphere, the temperature when full relative density is reached increases substantially (see Fig. 2), rendering viscosity and hence, σ_{100}, too low to cause type II cracks even at low heating rates. Conversely, for film pyrolyzed in a more oxidizing atmosphere, σ_{100} is high enough to cause type II cracks at a smaller critical thickness (see Fig. 7).

The general conditions for pyrolysis cracking can now be summarized. At low heating rates, σ_{max} due to weight loss is too small to exceed σ_c. When the film approaches full relative density, σ_{100} increases abruptly, causing cracking. The relatively high density of such type II cracks suggests that many nucleation sites, possibly from crystallites or gas bubbles, are available at this stage. The relatively short length of such cracks further suggests that interfacial adhesion has improved so that crack propagation is more difficult (i.e., a higher K_{IC}). The above condition for type II cracking is most severe in oxidizing atmospheres where T_{100} is the lowest and, hence, σ_{100} the highest. At high heating rates, σ_{max} is high and causes type I cracks during pyrolysis. The number of crack nuclei, mostly dust particles or other foreign objects, is limited, so the crack density is much lower. When the film finally approaches full density, σ_{100} again increases but is less severe, because T_{100} is higher. Thus, no further type II cracking takes place.

(3) Scaling Relations for Pyrolysis Cracks

We have previously shown two scaling relations between crack spacing λ, film thickness h, and heating rate R. These are

$$\text{Type I} \qquad \lambda \sim h^{-0.83} R^{-0.59} \tag{3}$$

and

$$\text{Type II} \qquad \lambda \sim h^{-0.83} R^{0.37} \tag{4}$$

We have also replotted the data of critical thickness in Figs. 7 and 13 and found them to follow the scaling relations below, which are illustrated in Figs. 16(a) and (b).

$$\text{Type I} \qquad h_c \sim R^{-0.32} \tag{5}$$

and

$$\text{Type II} \qquad h_c \sim R^{0.19} \tag{6}$$

We will now attempt to rationalize these scaling relations, using our scenario of stress maxima at T_{max} (due to $\dot{\varepsilon}_{max}$ for type I cracks) and T_{100} (due to η_{100} for type II cracks). According to the fundamental condition for thin-film cracking based on energy consideration, Eq. (2), we can write

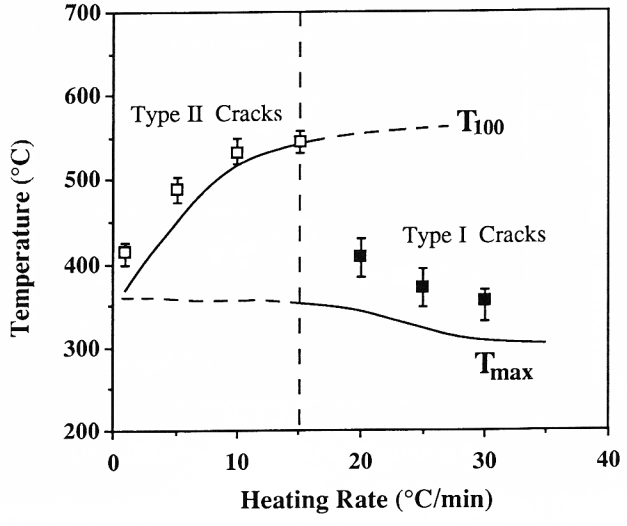

Fig. 15. First cracking temperature of BT films for type I cracks (closed symbols) and type II cracks (open symbols) at $h = 0.41$ μm. Also shown are T_{100} and T_{max}.

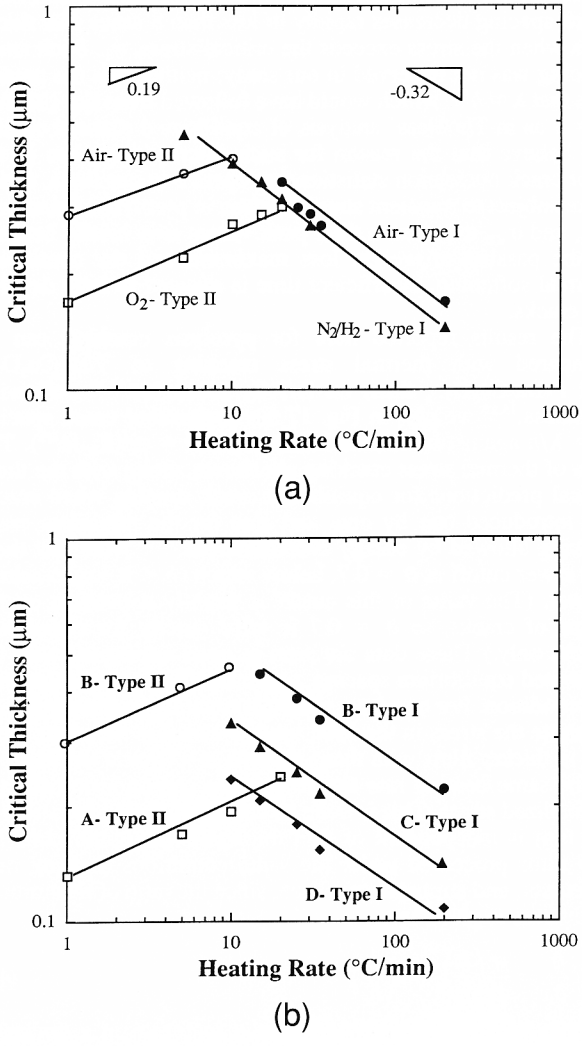

Fig. 16. Critical thickness vs heating rate for (a) BT films in different pyrolysis atmospheres, and (b) critical thickness vs heating rate for PZT films for various precursors (A–D). Type I cracks are shown in closed symbols and type II cracks in open symbols.

$$h_c \sim \frac{K_{IC}^2}{\eta^2 \dot{\varepsilon}^2} \tag{7}$$

by substitution of Eq. (1). Since type I and II cracks are associated with $\dot{\varepsilon}_{max}$ and η_{100}, respectively, we compare Eqs. (5) and (6) and Eq. (7) to conclude that

$$\dot{\varepsilon}_{max} \sim \sigma_{max} \sim R^{0.16} \tag{8}$$

and

$$\eta_{100} \sim \sigma_{100} \sim R^{-0.10} \tag{9}$$

These empirical dependencies are consistent with Fig. 14 for σ_{max} and σ_{100}. For crack spacing, scaling considerations dictate that the normalized crack spacing, λ/h, should be a function of $K_{IC}/\sigma h^{1/2}$, which is a measure of reciprocal strain energy normalized by fracture toughness. Writing

$$\frac{\lambda}{h} \sim \left(\frac{K_{IC}}{\sigma h^{1/2}}\right)^p \tag{10}$$

where p is an exponent, and substituting Eq. (1) for σ, we obtain

$$\lambda \sim \frac{K_{IC}^p}{\eta^p \dot{\varepsilon}^p h^{p/2-1}} \tag{11}$$

Comparing the thickness dependence of Eq. (11) with Eqs. (3) and (4), we conclude $p = 3.7$. It follows from Eqs. (8) and (9) that $\lambda \sim 1/\dot{\varepsilon}^p \sim R^{-0.59}$ for type I cracks and $\lambda \sim 1/\eta^p \sim R^{0.37}$ for type II cracks, in agreement with Eqs. (3) and (4). Thus, a self-consistent rationale of the scaling relations is found.

According to Thouless *et al.*,[15,25] equilibrium and minimum crack spacing decreases rapidly to less than 8 times film thickness when the stress exceeds the critical stress, σ_c. Such small spacing was not observed in our study; neither was the prediction that $\lambda \propto h^{1/2}$, which would have followed from Eq. (10) had $p = 1$ as in Thouless' analysis of equilibrated channel cracks. We believe that the reason for such discrepancies lies in the poor crack nucleation statistics that operate in our films, which were subject to transient stress maxima in pyrolysis. Since both σ_{max} and σ_{100} experience their peak values only briefly because of the passing of weight loss maximum and the continuing thermal softening, insufficient time is allowed to fully develop the cracks.

The results reported here for pyrolysis cracking can be compared with thermal stress cracking of $YBa_2Cu_3O_{7-x}$ and $PrBa_2Cu_3O_{7-x}$ films on $SrTiO_3$ substrates.[15,16] Following Thouless,[15,25] we plot in Fig. 17 the normalized crack spacing $\tilde{\lambda} = \lambda/h$ against normalized film stress $\tilde{\sigma} = \sigma/(K_{IC}/h^{1/2})$. The data of thermal stress cracking are shown, along with the theoretical predictions for equilibrium crack spacing when cracks are introduced one by one, and also for the minimum crack spacing allowed by energy considerations.[15–25] Note that there is a lower cutoff at $\tilde{\sigma} = 0.7$, below which ($h < h_c$) no cracking occurs. (The value of this cutoff is slightly dependent on the shape of cracks, so $\tilde{\sigma} = 0.7$ is valid strictly for channeling cracks only.) These data are seen in good agreement with the predicted equilibrium spacing, approaching $\lambda = 8h$ at the critical condition. For our data, although we are not able to directly estimate the stress in the film, we can compare the crack spacing in thicker films with those in films of a critical thickness h_c at the same heating rate and processing condition to infer the normalized stress. This is done by recognizing that the stress in the film is independent of film thickness and is the same for two films processed under the same conditions (heating rate, precursor, and atmosphere). Then, since the ratio of the normalized stress is given by

$$\frac{\tilde{\sigma}}{\tilde{\sigma}_c} = \frac{\sigma}{\sigma_c}\left(\frac{h}{h_c}\right)^{1/2} = \left(\frac{h}{h_c}\right)^{1/2} \tag{12}$$

and $\tilde{\sigma}_c = 0.7$, $\tilde{\sigma}$ for each data point in Fig. 6 at a thickness above h_c is simply 0.7 $(h/h_c)^{1/2}$. In this way, we are able to estimate $\tilde{\sigma}$ for both type I and type II cracks in $BaTiO_3$. These data are plotted, along with the normalized crack spacing which we measured directly, in Fig. 17. Note that the slopes of our data are around 3.6, which is the same as p in Eq. (10). This is self-consistent, because Eq. (10) is itself a relation between normalized spacing and normalized stress. Also note that these data are all clustered near the critical cracking boundary. This is consistent with our observation that the normalized crack spacing of pyrolysis cracks is much larger than that of thermal cracks, since at the critical cracking condition, the crack spacing necessarily diverges to infinity.

(4) Role of Precursors and Stoichiometry

Although the cracking conditions vary considerably with precursors, stoichiometry, and atmospheres, scaling relations (Eqs. (3–6)) are generally obeyed for various films pyrolyzed under different conditions. (See Figs. 10, 11, and 16.) This suggests that the cracking mechanisms and stress scenario are of a similar nature, and the role of precursors and stoichiometry can be rationalized within the same context. For $Pb(Zr_{1-x}Ti_x)O_3$ films, only type I cracks were seen in film from precursors B, C, and D for most heating rates, and the tendency for cracking increased in the above order. In films from precursor A, only type II cracks were seen for most heating rates, although they also appeared, but less severely, in films from precursor B. Table II summarizes the thermogravimetric characteristics of those precursors. Since the weight loss rate that is most relevant to type I cracks decreases in the order D, C, B, and A, it explains the decreasing tendency for type I cracks in the above systems. Indeed, in A the weight loss rate is probably too low to induce sufficient stress to cause type I cracks. It is also clear that the reason for the increasing maximum weight loss rate is due primarily to the sharpening of the peak (i.e., smaller ΔT) in precursors with increasing alkoxide content and decreasing carboxylate content. For type II cracks, Table I shows that the higher total carbon content in precursors A and B may be the cause. Very likely, some residual carbon remains in ceramic films even after approaching full relative density. For example, as reported by Lipeles *et al.*,[21] the ethylhexanote was not completely removed from the thin films after calcination at 400°C. Since the final oxidation of such residual carbon in the rigid, brittle ceramic matrix is likely to be the ultimate physical cause for strain and hence stress for type II cracks, a higher carbon content will likely increase the amount of residual carbon. This explains the observed carbon dependence. Lastly, the observed compositional effect regarding Zr/Ti ratio (Section III(6)) is also reasonable. The Zr-rich composition pyrolyzes slower,[19] thereby avoiding type I cracks and exhibiting only type II cracks.

In summary, films prepared by metallorganic decomposition methods are prone to formation of type II cracks when near

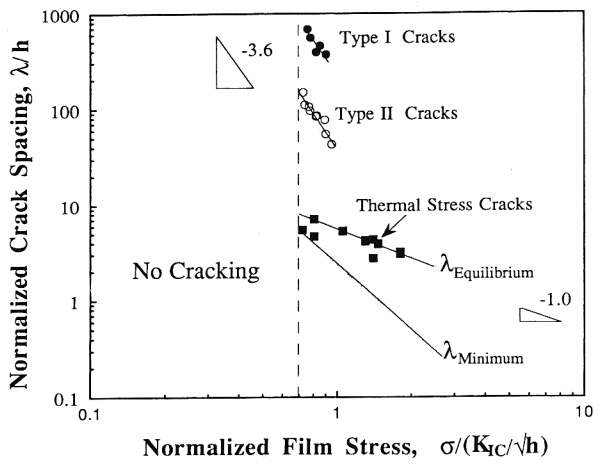

Fig. 17. Comparison of pyrolysis cracks of this study and thermal stress cracks of Thouless *et al.*[15,16] with theoretical predictions for equilibrium crack spacing and minimum crack spacing.[15,25] Data of crack spacing and film stress are shown in normalized form. No cracking occurs when $\sigma \leq \sigma_c$, corresponding to a normalized stress ≤ 0.7.

Table II. Thermogravimetric Characteristics of $Pb(Zr_{0.52}Ti_{0.48})O_3$ Precursors*

Precursor system	ΔW (%)	ΔT (°C)	$\Delta W/\Delta T$ (%/min)	"C" (wt%)
Precursor A Pb 2-ethylhexanoate Zr-2-ethylhexanoate Ti-diethoxy-dineodecanoate	62.1	325	2.86	44
Precursor B Pb 2-ethylhexanoate Zr-2-ethylhexanoate Ti-ethoxide	61.7	300	3.09	36
Precursor C Pb 2-ethylhexanoate Zr-n-propoxide Ti-ethoxide	55.9	220	3.81	26
Precursor D Pb-acetate Zr-n-propoxide Ti-ethoxide	31.7	110	4.32	14

*ΔW: Total weight loss excluding solvent. ΔT: Temperature range when weight loss occurs. "C": Total carbon content (in wt%) in raw precursors.

completion of pyrolysis. In contrast, films prepared by alkoxide sol–gel methods are prone to formation of type I cracks when the weight loss rate passes through a maximum. The systematic variation between the above two extremes can be rationalized by our understanding of stress development. In practice, by combining the thermogravimetric characteristics of these two extremes through precursor chemistry, we may obtain considerable freedom in tailoring pyrolysis characteristics and, hence, cracking resistance.

V. Conclusions

(1) Thin-film stresses develop in pyrolysis in two stages: first, at an intermediate temperature, when the maximum weight loss rate is experienced, then toward completion of pyrolysis. Type I cracks form at the first stage with a morphology similar to that seen in dried mud or on cracked glaze. Type II cracks form at the second stage with a morphology of starlike, short cracks.

(2) The maximum stress in stage I responsible for type I cracking is proportional to the strain (weight loss) rate, with an empirical dependence on the heating rate $\sigma \sim \dot{\varepsilon} \sim R^{0.16}$. The corresponding type I cracks are predominant under less oxidizing atmospheres, higher heating rates, and in films made by alkoxide sol–gel methods. The critical thickness scales with $R^{-0.32}$ and the crack spacing scales with $h^{-0.83} R^{-0.59}$.

(3) The maximum stress in stage II responsible for type II cracking is proportional to the viscosity, with an empirical dependence on the heating rate $\sigma \sim \eta \sim R^{-0.10}$. The corresponding type II cracks are predominant under oxidizing atmospheres, lower heating rates, and in films made by MOD methods. The critical thickness scales with $R^{0.19}$, and the crack spacing scales with $h^{-0.83} R^{0.37}$.

(4) Pyrolysis cracking is often limited by the availability of crack nuclei and the transient nature of stress maximum. Since it typically occurs near the critical cracking condition, its crack spacing is much larger than strain energy/fracture energy equilibration would allow. The nucleation sites of type I cracks are at dust/foreign particles. The nucleation sites of type II cracks are likely to be degassing bubbles and crystallite particles. The density of type II cracks, if they form, is much higher than that of type I cracks.

(5) Maximum thickness of about 0.4 μm of crack-free single coating films can be obtained in both $BaTiO_3$ and PZT films.

References

[1]R. A. Lipeles, D. J. Coleman, and M. S. Leung, "Effects of Hydrolysis on Metallo-organic Solution Deposition on PZT Films," *Mater. Res. Soc. Symp. Proc.*, **73**, 665–70 (1986).

[2]R. W. Vest, "Metallo-Organic Decomposition (MOD) Processing of Ferroelectric and Electro-Optical Films: A Review," *Ferroelectrics,* **102**, 53–68 (1990).

[3]J. Fukushima, K. Kodaira, and T. Matsushita, "Preparation of Ferroelectric PZT Films by Thermal Decomposition of Organometallic Compounds," *J. Mater. Sci.*, **9**, 595–98 (1984).

[4]K. D. Budd, S. K. Dey, and D. A. Payne, "Sol–Gel Processing of $PbTiO_3$, $PbZrO_3$, PZT and PLZT Thin Films," pp. 107–21 in *Br. Ceram. Proc.*, **36**, 107–21 (1985).

[5]S. L. Swartz, S. D. Ramamurth, J. R. Busch, and V. E. Wood, "Sol–Gel PZT Films for Optical Waveguides," *Mater. Res. Soc. Symp. Proc.*, **243**, 533–43 (1992).

[6]G. Yi and M. Sayer, "Sol–Gel Processing of Complex Oxide Films," *Am. Ceram. Soc. Bull.*, **70** [7] 1173–79 (1991).

[7]R. W. Vest and J. Xu, "$PbTiO_3$ Films from Metallo-organic Precursors," *IEEE Trans. Ultrason., Ferroelectr., Freq. Control*, **35** [6] 711–17 (1988).

[8]T. J. Garino, "The Cracking of Sol–Gel Films during Drying," *Mater. Res. Soc. Symp. Proc.*, **180**, 497–502 (1990).

[9]G. Yi, Z. Wu, and M. Sayer, "Preparation of $Pb(Zr,Ti)O_3$ Thin Films by Sol Gel Processing: Electrical, Optical and Electro-Optic Properties," *J. Appl. Phys.*, **64** [5] 2717–23 (1988).

[10]I. H. Pratt and C. Firestone, "Fabrication of RF-Sputtered Barium Titanate Thin Films," *J. Vac. Sci. Technol.*, **8** [1] 256–60 (1971).

[11]J. Xu, A. S. Shaikh, and R. W. Vest, "High K $BaTiO_3$ Films from Metallo-organic Precursors," *IEEE Trans. Ultrason., Ferroelectr., Freq. Control*, **36** [3] 307–11 (1989).

[12]A. S. Shaikh and G. M. Vest, "Kinetics of $BaTiO_3$ and $PbTiO_3$ Formation from Metallo-organic Precursors," *J. Am. Ceram. Soc.*, **69** [9] 682–88 (1986).

[13]S.-Y. Chen and I-W. Chen, "Temperature–Time–Texture Transition of $Pb(Zr_{1-x}Ti_x)O_3$ Thin Films: I, The Role of Pb-rich Intermediate Phases," *J. Am. Ceram. Soc.*, **77** [9] 2332–36 (1994).

[14]J. J. Ritter, R. S. Roth, and J. E. Blendell, "Alkoxide Precursor Synthesis and Characterization of Phases in the Barium Titanium Oxide System," *J. Am. Ceram. Soc.*, **69** [2] 155–62 (1986).

[15]M. D. Thouless, E. Olsson, and A. Gupta, "Cracking of Brittle Films on Elastic Substrates," *Acta Metall. Mater.*, **40** [6] 1287–92 (1992).

[16]E. Olsson, A. Gupta, M. D. Thouless, and A. Segmuller, "Crack Formation in Epitaxial [110] Thin Films of $YBa_2Cu_3O_{7-\delta}$ and $PrBa_2Cu_3O_{7-x}$ on [110] $SrTiO_3$ Substrates," *Appl. Phys. Lett.*, **58** [15] 1682–84 (1991).

[17]A. Atkinson and R. M. Guppy, "Mechanical Stability of Sol–Gel Films," *J. Mater. Sci.*, **126**, 3869–73 (1991).

[18]R. M. Guppy and A. Atkinson, "The Cracking Behaviour of Sol–Gel Films," *Br. Ceram. Proc.*, **49** [Spec. Ceram. 9] 203–14 (1992).

[19]S.-Y. Chen and I-W. Chen, "Temperature–Time–Texture Transition of $Pb(Zr_{1-x}Ti_x)O_3$ Thin Films: II, Heat Treatment and Compositional Effects," *J. Am. Ceram. Soc.*, **77** [9] 2337–44 (1994).

[20]T. J. Gardner and G. L. Messing, "Preparation of MgO Powder by Evaporative Decomposition of Solutions," *Am. Ceram. Soc. Bull.*, **63** [12] 1498–504 (1984).

[21]R. A. Lipeles, N. A. Ives, and M. S. Leung, "Sol–Gel Processing of Lead Zirconate Titanate Films"; pp. 320–26 in *Ultrastructure Processing of Ceramics, Glasses and Composites*. Edited by L. L. Hench and D. R. Ulrich. Wiley, New York, 1986.

[22]Y. Masuda, R. Ogawa, and Y. Kawate, "Preparation of $YBa_2Cu_3O_{7-x}$ Superconducting Films through the Sol–Gel Method Using Alkoxides as Starting Materials," *J. Mater. Res.*, **7** [4] 819–26 (1992).

[23]M. E. Gross, M. Hong, S. H. Liou, P. K. Gallagher, and J. Kwo, "Versatile New Metallo-organic Process for Preparing Superconducting Thin Films," *Appl. Phys. Lett.*, **52** [2] 160–62 (1988).

[24]J. W. Hutchinson and Z. Suo, "Mixed Mode Cracking in Layered Materials," *Adv. Appl. Mech.*, **29**, 63–174 (1991).

[25]M. D. Thouless, "Crack Spacing in Brittle Film on Elastic Substrates," *J. Am. Ceram. Soc.*, **73** [7] 2144–46 (1990). □